

NUMERICAL SIMULATION OF GENERAL RELATIVISTIC STELLAR COLLAPSE

CRISTIÁN R. GHEZZI AND PATRICIO S. LETELIER

*Instituto de Matemática Estatística e Computação Científica
Universidade Estadual de Campinas (UNICAMP-IMECC),
Cidade Univesitária, Barão Geraldo, 13083-859,
Campinas, São Paulo, Brazil
E-mail: ghezzi@ime.unicamp.br*

We present preliminar results and tests of a new general relativistic code to simulate the hydrodynamic collapse of a 21 solar masses star. We have assumed spherical symmetry and used the formalism of Misner and Sharp to construct a finite-difference scheme to solve the Einstein's equations, energy-momentum conservation equations and baryonic conservation equation. The code is similar to the one originally developed by May and White (1967). Here we discuss the capabilities of the code that make it well suited for numerical relativity on a personal computer and some caveats based on the experiments we have made with it.

1. Introduction

In this work we have reproduced the code of May and White (1967) (hereafter MW) using the same numerical techniques (with some little modifications) known from their pioneering work. We had also tested some modifications suggested by Van Riper (1979) (hereafter VR). The output of our code can be used as an initial Cauchy data for more sophisticated relativistic codes (see for example Baumgarte et al. 1995). The code developed here although based on old numerical techniques is simple to implement and little time consuming, which make it best suited for general relativistic simulations on a single personal computer. Here we briefly resumé the numerical caveats on a simulation of the hydrodynamic collapse of a 21 solar masses star that forms a black hole. The complete results of astrophysical interest will be published elsewhere (Ghezzi & Letelier 2003).

2. Numerical methods and initial conditions

We initially assumed uniform density perfect fluid balls, with adiabatic equation of state $P = K\rho^\gamma$, where γ is the adiabatic coefficient which is set equal to 5/3. It is also possivel to implement other equations of state in our code. The initial configuration resembles a newtonian star or a newtonian star-core collapsing under the gravity when nuclear fuel is exhausted. During the time evolution a strong field regime is achieved during which a neutron star or a black hole (a trapped surface)

may be formed depending on the initial conditions. The formation of the black hole was checked by the collapse of the g_{tt} metric coefficient (collapse of the “lapse function”). Alternatively, the black hole formation could be checked by observing the convergence of the light ray paths that pass near a Lagrangian coordinate μ , such that $2GM(\mu)/Rc^2 \geq 1$.

It is possible to assume arbitrary density or energy profiles as initial data sets, although we must observe that could be troublesome if discontinuities are present on the initial data.

We have used a Lax-Wendroff scheme (two step Richtmyer’s version) coupled with a Crank-Nicolson (1947) algorithm to solve the system of equations (similar to the techniques described in MW, and in VR). We have made tests using the viscosities given in VR and in MW. The boundary conditions are that the pressure is zero at surface, the mass of the star is zero at the centre of the star, and the coefficient g_{tt} of the metric is equal to one at the surface of the star. This last boundary condition assures that the coordinate time are synchronised with the clock of a comoving observer at the surface of the collapsing star. The results obtained from one run test are shown in the figures (a)-(d).

A novelty feature of our code is that it don’t break down when a black hole forms. This is because the code was built to self-adjust the time step in order to get the desired accuracy, and eventually the time step becomes exceedingly small when a black hole is obtained as the final outcome of the simulation. The code is very fast and accurate.

3. Discussion and Conclusion

Using the VR viscosity or the MW viscosity seems to give no different results using a low number of radial zones (~ 70). However, when a larger number of zones is set the MW viscosity seems to work better if it is multiplied by some constant factor greater than one. This is necessary to enlarge the shock waves through the zones, because when a large number of radial zones is used the shocks have a steeper representation, and this in turns could lead to numeric dispersion and consequently to a low accuracy.

It is possible to make very fast simulations, in the present case for example, using 200 radial zones the code take $\sim 10 - 30$ minutes to run on a Pentium IV, 1.7 Mhz. Although, to go further in the time evolution of the collapse could take much more time. The total accuracy at the end of the simulation is $\sim 99.5\%$. However, depending mostly on the choice of the viscosity parameter the accuracy could be worst.

We must point out that the code only depart from excellent energy conservation only when a trapped surface begins to form, so we think the precision obtained is quit satisfactory.

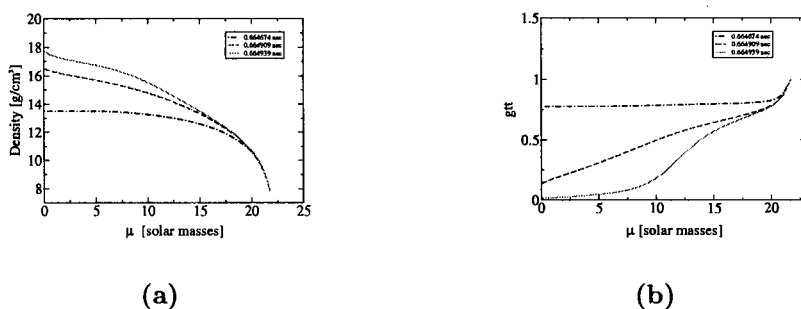


Figure 1. The figures displays a time sequence of snapshots as a function of the Lagrangian coordinate μ for the density (Fig. a), and for the metric coefficient g_{tt} (Fig. b).

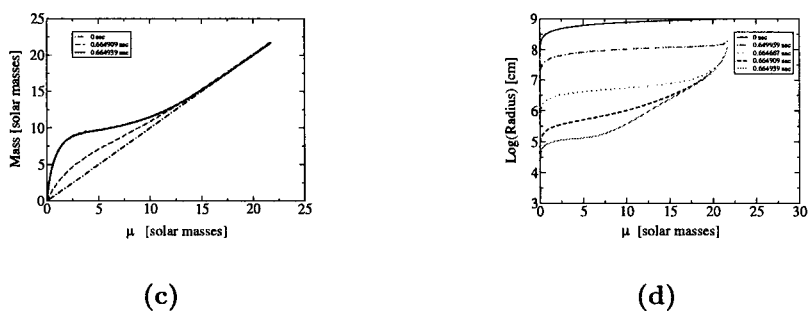


Figure 2. Snapshots for the total mass or energy (Fig. c), and for the radius of the configuration (Fig. d).

Acknowledgments

The authors acknowledge the brazilian agencies FAPESP, CNPQ and CAPES for support. CRG specially acknowledge FAPESP for additional support for the Tenth Marcel Grossmann meeting in Rio de Janeiro (2003).

References

1. Baumgarte T. W., Shapiro S. L., & Teukolsky S. A., ApJ (1995), **443**, 2,717-734.
2. Crank J., & Nicolson P., Proc. Cambridge Phil. Soc., **43**, 50 (1947).
3. Ghezzi C. R., & Letelier P. A. S., (2003) in preparation.
4. May M. M., & White R. H., Physical Review (1966), **141**, 4, (MW).
5. Misner C. W., & Sharp D. H., Pyhs. Rev. (1964), **136**, B571
6. Van Riper K. A., ApJ (1979), **232** 558-571, (VR).

TESTING BINARY BLACK HOLE CODES USING COSMOLOGICAL SPACE-TIMES

DAVID GARRISON

University of Houston - Clear Lake, 2700 Bay Area Blvd., Houston TX 77058, USA
E-mail: garrison@cl.uh.edu

In order to further our understanding of the instabilities which develop in numerical relativity codes, I study vacuum solutions of the cosmological type (T^3 topology). This involves testing the numerical code using the following non-trivial periodic solutions; Kasner, Gowdy, Bondi and non-linear gauge waves. I look for constraint violating and gauge mode instabilities and study numerical convergence. I will discuss techniques developed to investigate the stability properties of the numerical code.

1. Introduction

The goal of this project is to develop a technique of testing the stability of numerical relativity codes which may utilize any system for evolving Einstein's Equations. For the results presented here, I use this technique to test a Cactus Thorn^{1,2} based on the standard ADM evolution system using iterated Crank-Nicholson as a time integrator.

An unstable system is classically defined as one where any perturbation of the exact solution diverges as time increases until the numerical solution no longer depends on the initial data. Because an evolution can survive almost infinitely long before this happens, this definition is not always practical. For this reason, I begin by using a more precise definition of a stable or unstable numerical evolution. I refer to an evolution run as type 1 unstable if 1) the solution becomes discontinuous, 2) the space-time becomes unphysical, 3) the L2 norm of the numerical errors grows exponentially or 4) the L2 norm of the constraint errors grow exponentially. A type 1 unstable evolution is therefore one which appears obviously unstable to the casual observer. I refer to a system as type 2 unstable if it is defined as unstable according to the Lax-Richtmyer theorem³, which means that the numerical errors are not reduced with increasing resolution. If an evolution system can consistently produce both type 1 and type 2 unstable modes, we can consider that system to be numerically unstable. Meanwhile a stable evolution is one which can be defined as neither type 1 or type 2 unstable.

2. The Test

In order to develop an effective test for different numerical evolution systems it is important to first eliminate all possible causes of numerical instabilities outside of the evolution system itself. I use cosmological spacetimes in order to avoid black hole type singularities. This eliminates the need for singularity avoiding slicing conditions or special excision techniques. I also use periodic boundary conditions to avoid errors and reflections at the boundaries. Given a space-time with these properties, I try to stimulate gauge and constraint violating type 1 unstable modes and look for type 2 instabilities.

The general form of a diagonal four metric which lacks singularities and is periodic can be written as,

$$ds^2 = -\alpha(x,t)^2 dt^2 + e^{M(x,t)} dx^2 + e^{N(x,t)} dy^2 + e^{P(x,t)} dz^2. \quad (1)$$

With the appropriate choice of $\alpha(x,t)$, this basic metric can be modified to form any periodic diagonal solution to Einstein's equations. In the case where $\alpha = 1$, $M = N = P = 0$, the result is simply a flat space metric. If M , N and P are constant in x but not in time and $\alpha = 1$, the result is a Kasner spacetime. If α , M , N and P are periodic in x but not in time we get the Gowdy spacetime. If N and P are periodic in x and t but $M = 0$ and $\alpha = 1$, the result is a plane gravitational wave. This spacetime can only be periodic for the linearized form of Einstein's equations and is then called a Bondi Wave. The last possibility is that flat space is coordinate transformed so $N = P = 0$ and M and α are both periodic in x and time. The result is what appears to be a longitudinal gravitational wave or "gauge" wave.

3. Results

The linear systems, Kasner and Bondi, became type 1 unstable and produced constraint violating modes when a poor choice of lapse was introduced. The nonlinear systems, Gowdy and "gauge" wave, became type 1 unstable when large amplitude waves were used within the solution. Every run which became type 1 unstable also proved to be type 2 unstable. Only flat space-time evolutions appeared to be unconditionally stable. A Fourier analysis of the unstable runs seems to suggest that the instabilities may be caused by the increasingly large relative amplitudes of high frequency modes as resolution is increased.

4. Conclusion

The ADM evolution system appears to produce constraint violating modes when a poor choice of gauge is made. This system also produces gauge modes when large nonlinearities are introduced. Because of this, the ADM system is unlikely to be suitable for evolving binary black hole systems where different gauge choices and large nonlinearities may become essential. In order to determine which system should be used for binary black hole evolutions, I propose that these tests be used on some of the new hyperbolic numerical evolution systems^{4,5,6,7,8}.

5. Acknowledgements

The author acknowledges support by Penn State's Academic Computing Fellowship and grants NASA NGT5-127 and Sloan A P FDN 97-5-1AP. I would also like to thank LSU's numerical relativity group for their input.

References

1. The Cactus Development Team. *The Cactus Computational Toolkit*. <http://www.cactuscode.org>.
2. Erik Schnetter. *The Maya Project: General Concepts*, 2000. <http://www.eps.org/aps/meet/APR01/baps/abs/S1500041.html>.
3. Lloyd N. Trefethen. Finite Difference and Spectral Methods for Ordinary and Partial Differential Equations. <http://web.comlab.ox.ac.uk/oucl/work/nick.trefethen/pdetext.html>.
4. T. W. Baumgarte and S. L. Shapiro. *Phys.Rev.D59:024007*, 1999.
5. S. Frittelli and O. Reula. *J.Math.Phys.40:5143-5156*, 1999.
6. P. Laguna and D. Shoemaker. gr-qc/0202105.
7. L. E. Kidder, M. A. Scheel, and S. A. Teukolsky. *Phys.Rev.D64:064017*, 2001.
8. M. Shibata and T. Nakamura. *Phys.Rev.D52:5428-5444*, 1995.

THE SMOOTHNESS OF NULL INFINITY: ITS RELEVANCE FOR NUMERICAL RELATIVITY

J.A. VALIENTE KROON

Institut für Theoretische Physik der Universität Wien, Boltzmannsgasse 5, A-1090 Vienna, Austria. E-mail: jav@ap.univie.ac.at

The conformal approach to the description of isolated systems in General Relativity based on the notion of asymptotic simplicity usually assumes that the conformal boundary —null infinity— is a smooth submanifold. Some work on the so-called polyhomogeneous spacetimes has shown that much of the standard formalism holds on much weaker assumptions on the smoothness of null infinity. Furthermore, some recent work has shown that developments of Misner and Brill-Lindquist data have a non-smooth boundary. The latter raises the questions regarding the suitability of smooth null infinity to model "realistic" systems as different assumptions of the smoothness of the conformal boundary would yield slightly different physical predictions. This is an issue that is not only of relevance not for numerical simulations based on the conformal approach but in general for any code simulating asymptotically flat systems as some sort of asymptotic behaviour must at any rate be prescribed in order to model the "isolatedness" of the system. This prescribed asymptotic behaviour will contain implicit and explicit assumptions regarding the smoothness of null infinity. The relation between hyperboloidal initial data and Cauchy initial data is discussed within this context.

1 Isolated systems in General Relativity

We want to describe the Physics of isolated systems in General Relativity. Many of these systems can be treated by resorting only to the vacuum field equations. In order to characterise an isolated system one has to postulate some appropriate boundary (asymptotic) behaviour for the fields. Intuitively, these isolated systems should be "Minkowskian" in some appropriate sense. How to make more precise this idea? A way to proceed is by means of the notion of *asymptotic simplicity*. The crucial point —as seen by Penrose— is the following ^{1,2},

Proposal (Penrose, 1963, 1965). *Far fields of isolated systems behave like asymptotically simple spacetimes in the sense that they can be smoothly extended to null infinity after a suitable conformal rescaling.*

This approach has some clear advantages: null infinity is an idealisation of timelike observers; there is a rich framework to discuss gravitational radiation —polarisations states, extraction of wave forms, mass loss due radiative processes. All of these are uniquely defined via a Universal structure (null infinity). The quantities of relevance can be known by evaluating them at null infinity. There is no need of taking limits.

In the spirit of the proposal, the smoothness of null infinity is meant to convey a deep physical meaning. It is postulated as a property characterising isolated systems. If null infinity is smooth, then the gravitational field admits Taylor-like expansions in terms of the conformal factor Ω . If null infinity is not smooth but only C^k , then the asymptotic expansions may contain terms of the form,

$$\Omega^n \ln \Omega.$$

These expansions are known as *polyhomogeneous* —see e.g. ³.

A model with a polyhomogeneous null infinity and one with a smooth null infinity do produce different measurable effects. The wave forms would be in principle the same, however, a gyroscope located in the asymptotic region would precess differently depending on the model ⁴.

2 Importance of spatial infinity

H. Friedrich has constructed an existence proof for the so-called hyperboloidal initial value problem ⁵. This has been exemplified numerically by Hübner ⁶.

Recent developments on the constraint equations by Corvino allow us to construct initial data sets which are arbitrary inside a compact set, and Schwarzschildian outside it ⁷. These techniques can be used to —abstractly— construct spacetimes with a smooth null infinity. From this Cauchy data one can construct hyperboloidal data of arbitrarily small mass —i.e. close to Minkowski hyperboloidal data. Friedrich’s semiglobal existence results for hyperboloidal data then allow to recover the rest of the spacetime ⁸. Now, the location of the hyperboloids with respect to spatial infinity is irrelevant for Friedrich’s theorem. The latter fact indicates that the decision of having a smooth null infinity is made at spatial infinity. In order to analyse the problem further one requires a technique that allows to relate properties of null infinity with properties of the initial data. Such techniques have been developed by Friedrich ⁹.

Consider a simplified situation: time symmetric, conformally flat (e.g. Misner or Brill-Lindquist data). The use of Friedrich techniques yields the following ^{10,11,12},

Theorem (Valiente Kroon, 2002). *A time symmetric conformally flat initial data set with smooth null infinity has vanishing Newman-Penrose constants.*

The Misner and Brill-Lindquist data have non-vanishing Newman-Penrose constants. They have a non-smooth null infinity! This “malaise” can be healed by using the Corvino-Chruściel-Delay technique: construct modified Brill-Lindquist/Misner data which contains the wormholes inside a compact region and that is Schwarzschildian outside it. It is to be expected that the modified data will yield a smooth null infinity. This example shows that still within the conformal treatment one has still ambiguities on how to define unambiguously isolated systems (i.e. in fixing the right asymptotic conditions). Are there relevant physical differences between the possible boundary choices —i.e. does it matter?

The latter results are part of a larger conjecture —see ^{11,12}:

Conjecture. *Time symmetric initial data sets will have a development with a smooth null infinity if and if they are asymptotically static.*

The conjecture provides a physical interpretation of asymptotic simplicity. It has implications on the behaviour of the sources at early, late times.

3 Hyperboloidal data coming from Cauchy data?

Generically, and hyperboloidal initial data will yield a development with a smooth null infinity. On the other hand, it is very likely that Cauchy data will have

developments with smooth null infinity if and only if they are asymptotically static/stationary. Is it true that “nice” hyperboloidal data set can be traced back to an initial data set that is asymptotically stationary? Probably not. Again, does it matter? Criteria to decide this are certainly desirable.

There is too much freedom in defining an isolated system in General Relativity. One would like a way of removing this freedom while knowing what one is doing. Penrose’s proposal and the notion of asymptotic simplicity provide a way of consistently removing this freedom. It may be a bit too restrictive, but it is the price one may have to pay for having a consistent framework.

Acknowledgments

This research is funded by a Lise Meitner fellowship (M690-N09) of the Fonds zur Förderung der Wissenschaftlichen Forschung, FWF, Austria. The CA calculations reported have been carried out in the computers of the Albert Einstein Institut, Max Planck Institut für Gravitationsphysik, Golm bei Potsdam, Germany.

References

1. R. Penrose. Asymptotic properties of fields and space-times. *Phys. Rev. Lett.*, 10:66, 1963.
2. R. Penrose. Zero rest-mass fields including gravitation: asymptotic behaviour. *Proc. Roy. Soc. Lond. A*, 284:159, 1965.
3. P. T. Chruściel, M. A. H. MacCallum, and D. B. Singleton. Gravitational waves in general relativity XIV. Bondi expansions and the “polyhomogeneity” of \mathcal{I} . *Phil. Trans. Roy. Soc. Lond. A*, 350:113, 1995.
4. J. A. Valiente Kroon. Can one detect a non-smooth null infinity? *Class. Quantum Grav.*, 18:4311, 2001.
5. H. Friedrich. On the existence of n-geodesically complete or future complete solutions of Einstein’s field equations with smooth asymptotic structure. *Comm. Math. Phys.*, 107:587, 1986.
6. P. Hübner. From now to timelike infinity on a finite grid. *Class. Quantum Grav.*, 18(1871), 2001.
7. J. Corvino. Scalar curvature deformations and a gluing construction for the Einstein constraint equations. *Comm. Math. Phys.*, 214:137, 2000.
8. P. T. Chruściel and E. Delay. Existence of non-riivial, vacuum, asymptotically simple spacetimes. *Class. Quantum Grav.*, 19:L71, 2002.
9. H. Friedrich. Gravitational fields near space-like and null infinity. *J. Geom. Phys.*, 24:83, 1998.
10. S. Dain and J. A. Valiente Kroon. Conserved quantities in a black hole collision. *Class. Quantum Grav.*, 19:811, 2002.
11. J. A. Valiente Kroon. A new class of obstructions to the smoothness of null infinity. in [gr-qc/0211024](#).
12. J. A. Valiente Kroon. Does asymptotic simplicity allow for radiation near spatial infinity? in [gr-qc/0309016](#).

COLLAPSE OF A DIFFERENTIALLY ROTATING SUPERMASSIVE STAR

MOTOYUKI SAIJO

*Department of Physics, Kyoto University,
Kyoto 606-8502, Japan
E-mail: saijo@tap.scphys.kyoto-u.ac.jp*

We investigate the gravitational collapse of rapidly rotating relativistic supermassive stars by means of a 3+1 hydrodynamical simulations in conformally flat spacetime of general relativity. We study the evolution of differentially rotating supermassive stars of $q \equiv J/M^2 \sim 1$ (J is the angular momentum and M is the gravitational mass of the star) from $R/M \sim 65$ (R is the circumferential radius of the star) to the point where the conformally flat approximation breaks down. We find that the collapse of the star of $q \gtrsim 1$, a radially unstable differentially rotating star form a black hole of $q \lesssim 1$. The main reason to prevent the formation of a black hole of $q \gtrsim 1$ is that quite a large amount of the angular momentum stays at the surface. We also find that the collapse is coherent and that it likely leads to the formation of a supermassive black hole with no appreciable disk nor bar. In the absence of nonaxisymmetric deformation, the collapse of differentially rotating supermassive stars are the promising sources of burst and quasinormal ringing waves in the Laser Interferometer Space Antenna.

There is increasing evidence that supermassive black holes (SMBHs) exist at the center of all galaxies, and that they are the sources which power active galactic nuclei and quasars. For example, VLBI observations of the Keplerian disk around an object in NGC4258 indicate that the central object has a mass $M \sim 3.6 \times 10^7 M_\odot$ and radius less than ~ 13 pc. Also, large numbers of observations are provided by the Hubble space telescope suggesting that SMBHs exist in galaxies such as M31 ($3 \times 10^7 M_\odot$), M87 ($1 \sim 2 \times 10^9 M_\odot$) and our own galaxy ($2.5 \times 10^6 M_\odot$). Although evidence of the existence of SMBHs is compelling, the actual formation process of these objects is still uncertain¹. Several different scenarios have been proposed, some based on stellar dynamics, others on gas hydrodynamics, and still others which combine the processes. At present, there is no definitive observation as yet which confirms or rules out any one of these scenarios.

Here we discuss the collapse of a supermassive star (SMS) as one scenario of formation of a SMBH. This subject is also interesting from the viewpoint of general relativity. The complete gravitational collapse of a body always results in a black hole (BH) rather than naked singularity, and the final state of the BH should go into the stationary one (the sequence of Kerr BHs) due to the uniqueness theorem. However there are several exceptions to this cosmic censor. BH uniqueness theorem

requires that the stationary BH always rotates less than the maximum Kerr limit; i.e. $J/M^2 \lesssim 1$. Therefore, a collapse of a star with the critical value $J/M^2 \sim 1$ (J is the angular momentum, M is the total gravitational energy) may show us a violent phenomenon in general relativity and in gravitational wave physics.

We perform the conformally flat simulations² for the following threefold. The first is to verify the nature of the gravitational collapse of a differentially rotating equilibrium star from the viewpoint of cosmic censor. The second is to determine the final outcome of the collapse of differentially rotating SMSs. Finally, it is important to probe whether the collapse of differentially rotating SMSs could be promising sources of gravitational waves.

We investigate the collapse of a differentially rotating SMS by means of hydrodynamic simulations in conformally flat approximation in general relativity. We start our collapse from $R/M \sim 65$, where R is the circumferential radius of the star, to the point where conformally flat approximation breaks down.

First we find that the cosmic censor conjecture even holds for gravitational collapse of radially unstable equilibrium star of $J/M^2 \gtrsim 1$. The main reason to prevent to form a BH of $J/M^2 \gtrsim 1$ is the transport of angular momentum to the surface. Note that even a thin disk near the surface of the star can hold relatively a large amount of angular momentum if the radius is large. (See Fig. 1 for the final distribution of “ J/M^2 ”.)

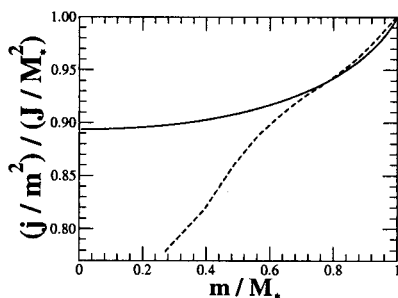


Figure 1. Profile of j/m^2 as a function of cylindrical mass m for Model II (Table 2 of Ref. [2]). Solid and dashed line denotes the profile at $t = 0$ and $t = 5.64 t_{\text{dyn}}$, respectively. Note that j is the cylindrical angular momentum, M_* is the rest mass, t_{dyn} is the dynamical time defined in Ref. [2].

Second, collapse of a differentially rotating, relativistically unstable SMS is coherent and likely leads to the formation of a SMBH. This situation is quite similar to the collapse of a uniformly rotating SMS³. Combining these two results, we conclude that collapse of a SMS is coherent within the order of dynamical time.

Third, we cannot find any evidence of bar formation nor significant disk formation from rotating collapse prior to BH formation. The phenomena of no bar

formation also comes from the fact that mass density collapses first to form a BH. In such case, T/W cannot scale in R^{-1} due to the growth of the degree of differential rotation, and as a fact the star of T/W cannot reach the dynamical instability criterion of ~ 0.27 . (See Fig. 2 for the final coordinate density contour in the equatorial plane.)

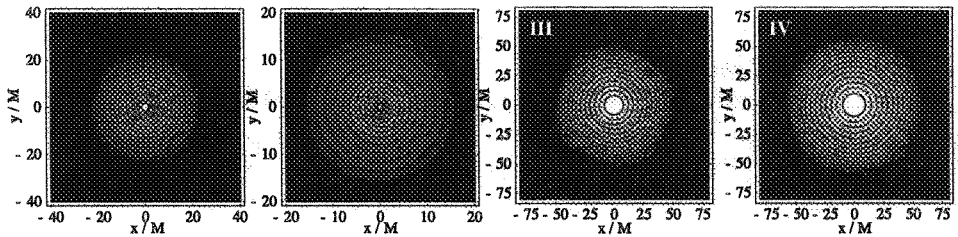


Figure 2. Final density contour in the equatorial plane of 4 differentially rotating stars. Model I, II, III, IV (Table 2 of Ref. [2]) is plotted at the parameter $(t/t_{\text{dyn}}, \rho_{\text{max}}^*) = (4.38, 1.37 \times 10^{-3})$, $(5.62, 2.16 \times 10^{-2})$, $(5.61, 9.13 \times 10^{-6})$, $(5.60, 5.33 \times 10^{-6})$, respectively. The contour lines denote coordinate densities $\rho^* = \rho_{\text{max}}^* \times 10^{-0.267(16-i)}$ ($i = 1, \dots, 15$).

Finally, rotating SMS collapse is a promising source of burst gravitational waves and of quasi-normal mode ringing waves. We can estimate the strength and the frequency of the wave burst and the wave quasinormal ringing emitted from this rotating collapse as $f_{\text{burst}} \sim 3 \times 10^{-2} (10^6 M_{\odot}/M) (M/R)^{3/2} [\text{Hz}]$. The wave amplitude can be estimated by employing the quadrupole formula according to $h_{\text{burst}} \sim 1 \times 10^{-18} (M/(10^6 M_{\odot})) (1 \text{Gpc}/d) (M/R)$, where Q is the quadrupole moment of the star and d is the distance from the observer. We set $R/M = 1$, a characteristic mean radius during BH formation. The characteristic frequency f_{QNM} and strength h_{QNM} of this radiation in rotating star collapse are $f_{\text{QNM}} \sim 2 \times 10^{-2} (10^6 M_{\odot}/M) [\text{Hz}]$, $h_{\text{QNM}} \sim 6 \times 10^{-19} ((\Delta E_{\text{GW}}/M)/10^{-4})^{1/2} (2 \times 10^{-2} [\text{Hz}]/f_{\text{QNM}})^{1/2} (M/(10^6 M_{\odot}))^{1/2} (1 \text{Gpc}/d)$, where ΔE_{GW} is total radiated energy. Since the main targets of LISA are gravitational radiation sources between 10^{-4} and 10^{-1} Hz, it is possible that LISA can search for the burst waves and the quasinormal ringing waves accompanying rotating SMS collapse and formation of a SMBH.

References

1. M. J. Rees, in *Black Holes in Binaries and Galactic Nuclei*, edited by L. Kaper, E. P. J. van den Heuvel, and P. A. Woudt (Springer-Verlag, New York), 351 (2001).
2. M. Saijo, Submitted to *Astrophys. J.* (2003).
3. M. Saijo, T. W. Baumgarte, S. L. Shapiro, and M. Shibata, *Astrophys. J.* **569**, 349 (2002).
4. K. S. Thorne, in *300 Years of Gravitation*, edited by S. Hawking and W. Israel (Cambridge Univ. Press, Cambridge, 1987), 330.

ANALYSING CURVED SPACETIMES WITH TENSOR SPLATS

WERNER BENGER*⁺

HANS-CHRISTIAN HEGE*

** Zuse Institute Berlin, Takustrasse 7, D-14195 Berlin-Dahlem
E-mail: benger@zib.de, hege@zib.de*

*⁺ Max-Planck-Institute for Gravitational Physics (Albert-Einstein-Institute),
Auf dem Muehlenberg 1, D-14467 Golm
E-mail: Werner.Benger@aei.mpg.de*

A new visualization technique for visualizing three-dimensional symmetric positive definite tensor fields of rank two is described. It supports studying the spatial projection of a spacetime metric. The rendering technique is demonstrated upon the Schwarzschild metric of a static black hole, the Kerr metric of a rotating black hole in two different coordinate systems, and a numerically computed dataset describing the metric of two colliding black holes.

1 Introduction and Motivation

Solutions of the Einstein equations are usually treated in a purely abstract mathematical way, i.e. as algebraic expressions. Determination of certain spacetime properties requires further calculation, for instance the computation of geodesic paths or isometric embeddings of certain slices of the spacetime. Penrose diagrams can be constructed for sufficiently known spacetimes and light cones are widely used to visualize the 4-metric at selected points. But these visualization methods can hardly cover an entire data volume at once. Direct visualization of the 3-metric is uncommon, because of limited availability of suitable visualization methods as well as minor experience in general relativity. However, in other scientific domains like material sciences as well as in computational fluid dynamics the direct visualization of tensor fields has a relatively long-grown history. Especially in medical sciences a strong interest on tensor field visualizations has advanced with the recent developments in magneto-resonance equipment which provide measurements of water diffusion within the human brain as tensor fields^{1,2,3,4,5}. These visualization techniques have in common the difficulty to display (at least) six independent quantities per point in a whole volume at the same time. Tackling the same problem for data sets from general relativity is desirably as well, on the one hand for the scientist who needs to inspect his data, e.g. from huge numerical simulations, quantitatively or qualitatively, on the other hand also for public outreach, which is especially difficult for an abstract scientific domain like general relativity.

2 Visualization Technique

A straightforward way to look at a tensor in a coordinate-independent way is to consider the set of tangential vectors $\vec{v} \in T_p(M)$ which are mapped to the same number $G(\vec{v}, \vec{v}) = C$ with $C \in \mathbb{R}$. By interpreting tangential vectors as small distances, we can interpret this set of tangential vectors as a set of points around a

certain point in space, therefore obtaining a quadric surface representing the tensor. This surface is an ellipsoid for positive definite tensors and an hyperboloid when negative eigenvalues occur. A quadric surface does not display the full information content of a general tensor, but only its symmetric part, which is sufficient for metric tensor fields. By definition the spatial projection of a spacetime metric is always positive definite, so a visualization method may assume positive definiteness.

An intuitively useful classification of tensor ellipsoids on behalf of their shapes was given by Westin ⁶. He introduced shape factors indicating the relationships among the three eigenvalues $\lambda_{max}, \lambda_{med}, \lambda_{min}$. They only depend on the ellipsoid shape, independent from its size:

$$c_l = \frac{\lambda_{max} - \lambda_{med}}{\lambda_{max} + \lambda_{med} + \lambda_{min}} \quad c_p = \frac{2(\lambda_{med} - \lambda_{min})}{\lambda_{max} + \lambda_{med} + \lambda_{min}} \quad c_s = \frac{3\lambda_{min}}{\lambda_{max} + \lambda_{med} + \lambda_{min}}.$$

The scaling numbers 2 and 3 are used such that each shape factor is in the interval $[0, 1]$. Other normalization choices are possible as well. The three shape factors obey the relationship $c_l + c_p + c_s = 1$ and can thus be interpreted as barycentric coordinates within a triangle, as illustrated in Fig. 1. The spherical factor c_s is a measure of the anisotropy.

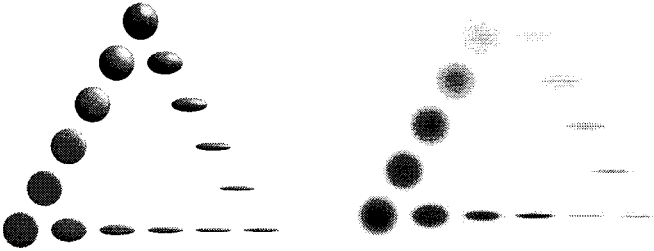


Figure 1. Ellipsoids (left) incorporating the tensor field's value at each point in space are substituted by transparent discs (right), which are equipped with an texturing to enhance linearity. The left edge corresponds to $c_l = 0$, bottom edge to $c_s = 0$ and the right edge to $c_p = 0$.

Now the idea of the tensor splat rendering technique is to simplify tensor ellipsoids by simplified version that incorporate the same information content, but allow rendering of a full three-dimensional volume due to their simpler shape. This technique is described in detail elsewhere ⁷. Here, we concentrate on the application of this rendering technique on general relativistic metrics.

3 Visualization of Metric Tensor Fields

3.1 Schwarzschild Metric

The famous Schwarzschild metric is known as

$$ds^2 = (1 - 2m/r) dt^2 - \frac{1}{1 - 2m/r} dr^2 - r^2 d\vartheta^2 - r^2 \sin^2 \vartheta d\varphi^2 \quad (1)$$

whereby for our visualization purposes we are only interested in the spatial part. We see immediately that the radial eigenvector $\vec{\partial}_r$ is dominant with eigenvalue $g_{rr} = 1/(1 - 2m/r) > 1$. The tensor field thus contains no linear but only planar regions, whereby the anisotropy is highest for $r \rightarrow 2m$ (the “event horizon” of the black hole). This behavior of radial stretching is easily depicted by the tensor splats, Fig. 2. as radially oriented planar discs (Fig. 2, right left) indicating light propagation. The co-metric (Fig. 2, rightmost) appears as radial “needles”, indicating the pure radial stretching toward the event horizon as well. While both images, the tensor and the inverse tensor, provide the same information content, it is still useful to be able to switch between both visual representations.

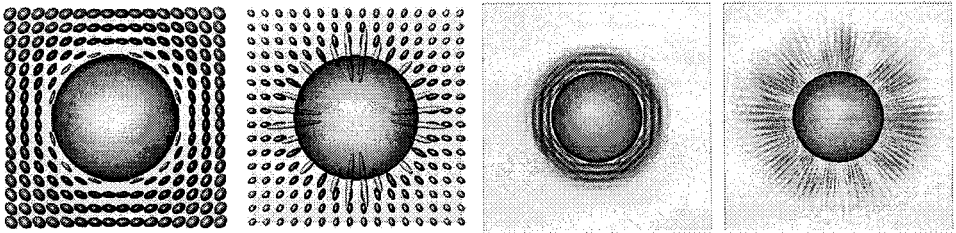


Figure 2. Tensor ellipsoids (left) and tensor splats (right) on a two-dimensional subspace of the Schwarzschild metric (first and third image) and its co-metric (second and fourth image). Note that the icons still represent the full three-dimensional metric. The region within the event horizon is not shown. The broken spherical symmetry in the rightmost image is due to the ambiguity of the minor and median eigenvalue in the Schwarzschild spacetime.

3.2 Kerr Metric

The Kerr metric describes a rotating black hole with mass m and angular momentum a . In matrix notation, the 4-metric reads in Boyer-Lindquist coordinates:

$$\begin{aligned}
 ds^2 = & \left(1 - \frac{2mr}{\varrho^2}\right) dt^2 + 2 \frac{mra \sin^2 \vartheta}{\varrho^2} dt d\varphi \\
 & - \frac{\varrho^2}{\Delta} dr^2 - \varrho^2 d\vartheta^2 - \frac{(r^2 + a^2) - \Delta a^2 \sin^2 \vartheta}{\varrho^2} \sin^2 \vartheta d\varphi^2
 \end{aligned} \tag{2}$$

whereby $\Delta := r^2 - 2mr + a^2$ and $\varrho^2 := r^2 + a^2 \cos^2 \vartheta$. The condition $a < m$ must hold for a physically reasonable black hole. The case $a = m$ is known as a maximally spinning black hole. For $a > 0$ the Kerr metric is no longer spherically symmetric, but just axially symmetric around the rotation axis. With increasing angular momentum, the tensor splat rendering exhibits the increase of axial linear stretching in the equatorial plane in a three-dimensional view of the Kerr metric, as demonstrated in reference ⁷. The spatial projection of a four-dimensional metric depends on the choice of the time coordinate. Boyer-Lindquist coordinates become singular at the horizons of the Kerr black hole, similar to the Schwarzschild coordinates. This coordinate singularity is avoided by Kerr-Schild coordinates, where

the spatial projection (the only relevant part for this visualization) is given by ⁸:

$$ds^2 = \left(1 + \frac{2mr}{\varrho^2}\right) dr^2 - \left[1 + \frac{2mr}{\varrho^2}\right] a \sin^2 \vartheta dr d\varphi + \varrho^2 d\vartheta^2 + \left[r^2 + a^2 + \frac{2mr}{\varrho^2} a^2 \sin^2 \vartheta\right] \sin^2 \vartheta d\varphi^2 \quad (3)$$

Displaying this spatial metric using ellipsoids yields an impression of a maelstrom of the spacetime, which is not prominent in the Boyer-Lindquist form. However, the Boyer-Lindquist simplifies reading off the geometrical properties of the spacetime, especially the linear stretching of the spacetime in the equatorial region.

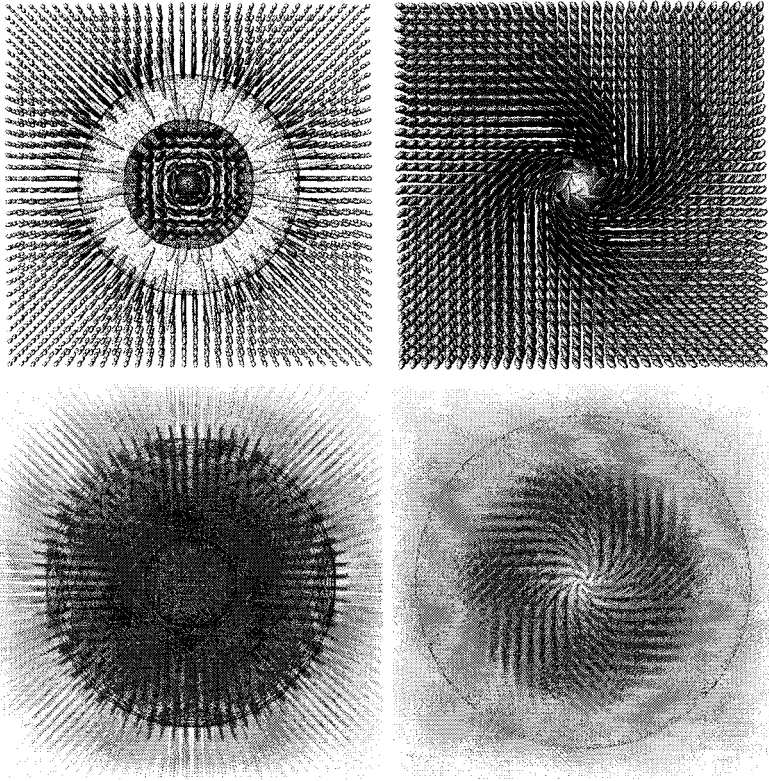


Figure 3. Comparison of the spatial part of the Kerr metric in Boyer-Lindquist (left column) and Kerr-Schild coordinates (right column), visualized by tensor ellipsoids (upper row) and tensor splats (lower row).

In comparison to the ellipsoid drawing, the tensor splat technique yields more brilliant images when operating on a full three-dimensional volume, as it suppresses less important information better than the ellipsoid technique. Still, the important information is conserved.

3.3 Numerical Data

Exact solutions of the Einstein equations are rare and no generic solution is known yet. Even the apparently simple two-problem, leading to the well known Kepler ellipses in the Newtonian theory, still withstands all attempts to find an exact solution and require numerical methods. In numerical relativity⁹, the spatial 3-metric is a primary computational quantity and the described visualization method provides a direct visualization of the computed data sets. Of special interest

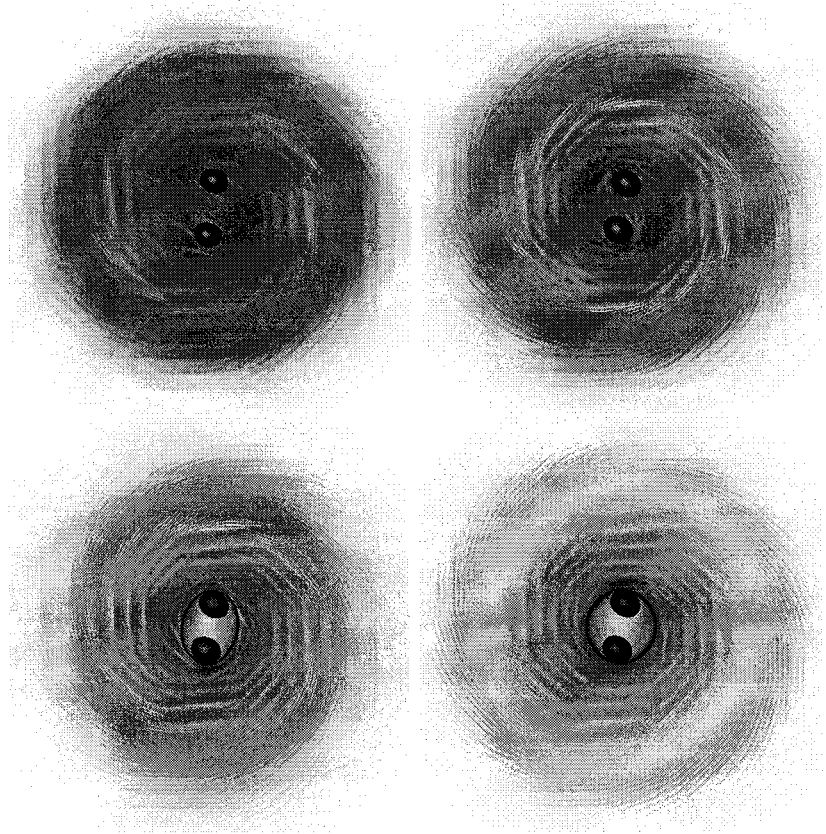


Figure 4. Snapshots from a numerical black hole merger sequence, depicting regions of highly linear grid stretching within regions of more planar grid stretching.

in numerical relativity is the occurrence of “grid stretching”, the locally varying physical distance between neighboring points on the numerical grid. Due to physical or coordinate singularities they lead to numerical instabilities, ultimately killing the entire simulation. Early detection of such instabilities is thus essential for the development of improved evolution schemes. Fig. 4 shows the tensor splats technique applied to selected time steps of a numerical evolution from two colliding, initially orbiting black holes. The $t \rightarrow \infty$ limit of such a collision process is known to be the Kerr metric (2). Although this result is not necessarily given in Boyer-Lindquist coordinates, the similarity to the Kerr-Schild appearance of the rotating black hole is obvious.

Acknowledgments

The visualization routines were implemented as an extension to the Amira ¹⁰ visualization environment. The data set of orbiting black holes was computed with Cactus ¹¹ by the numerical relativity group at the Max-Planck-Institute for Gravitational Physics in Potsdam, Germany, using computational resources at the National Center for Supercomputing Applications.

References

1. L. Zhukov, K. Museth, D. Breen, R. Whitaker, and A. Barr. Level set segmentation and modeling of dt-mri human brain data. *Journal of Electronic Imaging*, 12(1):125–133, 2003.
2. D.S. Tuch, T.G. Reese, M.R. Wiegell, N.G. Makris, J.W. Belliveau, and V.J. Wedeen. High angular resolution diffusion imaging reveals intravoxel white matter fiber heterogeneity. *Magn Reson Med.*, 48:577–582, 2002.
3. G. Kindlmann, D. Weinstein, and D. Hart. Strategies for direct volume rendering of diffusion tensor fields. *IEEE Transactions on Visualization and Computer Graphics*, 6(2):124–138, 2000.
4. C.F. Westin, S.E. Maier, B. Khidhir, P. Everett, F.A. Jolesz, and R. Kikinis. Image processing for diffusion tensor magnetic resonance imaging. In editors Taylor C, Colchester A, editor, *MICCAI 99: Second International Conference on Medical Image Computing and Computer-Assisted Intervention*, pages 441–452. Springer Verlag, Heidelberg, Germany, 1999.
5. S. Zhang and D. H. Laidlaw. Elucidating neural structure in diffusion tensor mri volumes using streamtubes and streamsurfaces. In *Proc. Intl. Soc. Mag. Reson. Med.*, number 9, 2001.
6. C.F. Westin, S. Peled, H. Gudbjartsson, R. Kikinis, and FA. Jolesz. Geometrical diffusion measures for mri from tensor basis analysis. In *Proceedings of ISMRM, Fifth Meeting, Vancouver, Canada*, page 1742, April 1997.
7. W. Bengler and H.-C. Hege. Tensor splats. In *to appear in Conference on Visualization and Data Analysis 2004*.
8. G. Cook. Initial data for numerical relativity. *Living Rev. Relativity*, 3(5), 2000. [Online article]: cited on 15 Aug 2001, <http://www.livingreviews.org/lrr-2000-5>.
9. G. Allen, T. Goodale, G. Lanfermann, E. Seidel, W. Bengler, H.-C. Hege, A. Merzky, J. Massó, and J. Shalf. Solving einstein’s equation on supercomputers. *IEEE Computer*, 32(12):52–59, December 1999. http://www.computer.org/computer/articles/einstein_1299_1.htm.
10. D. Stalling, M. Westerhoff, and H.-C. Hege. Amira - an object oriented system for visual data analysis. In Christopher R. Johnson and Charles D. Hansen, editors, *Visualization Handbook*. Academic Press, to appear 2004. <http://www.amiravis.com/>.
11. Max-Planck-Institute for Gravitational Physics. The cactus computational toolkit. <http://www.cactuscode.org/>, 2003.